Modeling of the keyhole asymmetry in dissimilar laser welding

I. Tomashchuk[1]*, J.-M. Jouvard[1], P. Sallamand[1], M. Duband[1]

[1] Laboratoire Interdisciplinaire Carnot de Bourgogne (ICB), UMR CNRS 6303- Université de Bourgogne – Franche Comté, 12, rue de la Fonderie – 71200 Le Creusot, France
* iryna.tomashchuk@u-bourgogne.fr

Abstract: An auto-consistent multiphysical 3D model with strong coupling between Heat Transfer, Navier Stokes and ALE problems is proposed for the description of transient development of the keyhole and the melted zone in laser welding of metallic materials. It showed a satisfactory correspondence with experimental melt dimensions in case of standalone and dissimilar pulsed laser welds and allowed an adequate representation of free surface evolution, comprising the advanced stages of evaporative digging of the keyhole and further cooling collapse. The model was used for the comprehension of keyhole asymmetry in the dissimilar joints, on the example of butt joints welded by a pulsed laser. The asymmetry of the keyhole between the reference metal and the neighboring random metal was quantified using two parameters: a relative keyhole section and a relative root offset in the reference material. Both parameters were increasing with the vaporization temperature of the neighboring material. However, for highly reflective materials this increase was much slower.

Keywords: laser, dissimilar welding, free surface, multiphysics.

1. Introduction

In deep penetration laser welding, the shape of vapor-filled keyhole is determinative for the development of the melted zone. In case of welding between the materials having a strong mismatch in physical properties, the keyhole can become asymmetrical, with its root more or less shifted away from the joint line [1,2]. Very few experimental studies were focused on the behavior of the keyhole in the dissimilar joint. On the crosscut macrographies of partial penetration laser welds between the metals with strong mismatch in vaporization temperature, such as titanium/tantalum[2], the shift of melted zone root from the joint line was clearly visible, which signifies the respective offset of the keyhole during the process. Torkamany et al [1], proved the keyhole asymmetry during niobium/titanium laser welding using top view observation by high-speed camera and metallographic cross-section examination: the keyhole was entirely shifted on titanium side that has lower vaporization temperature. Mostafa et al.[3,4] performed high speed imaging of a keyhole formed between aluminum A5754 and magnesium AZ31 alloys during a standalone laser pulse and reported the formation of the keyhole mainly on magnesium side that also has lower vaporization temperature. In the same time, the dissimilar welding that involves a highly reflective material such as copper in copper/steel joints [5] typically results in the formation of the keyhole shifted towards less reflective material. These two factors – vaporization temperature and absorption coefficient – seem to be determinative for the keyhole asymmetry as they define the competing vaporization fluxes on each side of the joint.

As the keyhole position to the joint line is a key factor of dilution between the dissimilar materials and therefore controls the final weld quality, it is important to comprehend the keyhole asymmetry for each individual welded couple. The numerical model of keyhole formation previously described in [6] was completed with evaporative heat loss term, which allowed more realistic representation of advanced stages of keyhole progression. After the validation on several materials and conditions, it was applied to the different dissimilar couples that have strong mismatch in physical properties, for the evaluation of the keyhole asymmetry in pulsed welding.

2. Governing equations

2.1. Heat transfer

Heat transfer equation was solved in time-dependent form

$$\rho C_p^{eq} \frac{\partial T}{\partial t} + \rho C_p^{eq} \overrightarrow{U} \cdot \overrightarrow{\nabla} T = \overrightarrow{\nabla} \cdot \left(k \overrightarrow{\nabla} T\right) \quad (1)$$

with ρ - local density (kg/m^3), C_p^{eq} – local equivalent heat capacity (J/(kg·K)), k – local thermal conductivity (W/(m·K)), T – solved temperature (K) and t – time (s).

The energy supply from a standalone laser pulse was introduced as top surface Gaussian heat source:

$$q_{laser} = \frac{2\, a\, P_l}{\pi\, {R_l}^2} exp^{-2\frac{(x^2+y^2)}{{R_l}^2}} \cdot \left(t \geq t_{imp}\right) \quad (2)$$

with a – local absorption coefficient of laser radiation, P_l – laser power (W), R_l – laser beam radius (m), and t_{imp} – the duration of laser pulse (ms).

The heat loss through evaporation was represented by top surface vaporization heat flux [7]:

$$q_{vap} = -(1-\beta_r) L_{vap} \sqrt{\frac{M}{2\pi RT}} P_{sat} \quad (3)$$

where β_r– the recombination coefficient, L_{vap} – local latent heat of vaporization (J/kg), M – molar mass (kg/mol), R – ideal gas constant (J/(mol·K)), P_{sat} – saturated vapor pressure (Pa).

The heat loss due to the interaction with environment was represented by convective heat flux:

$$q_{conv} = h(T_{amb} - T) \quad (4)$$

where h (W/(m²·K) - heat transfer coefficient and T_{amb} – ambient temperature (K).

For the lateral walls of the domain, thermal insulation was applied.

2.2. Fluid flow

The melted metal was considered as an incompressible Newtonian liquid with T-dependent dynamic viscosity μ (Pa·s) that undergoes time-dependent laminar flow governed by Navier-Stokes equation:

$$\rho \frac{\partial \vec{U}}{\partial t} + \rho(\vec{U} \cdot \overrightarrow{\nabla})\vec{U} = \overrightarrow{\nabla} \cdot \left\{p\, 2[I] + \mu \left[\nabla \vec{U} + \left(\nabla \vec{U}\right)^T\right]\right\} + \vec{F}_D + \rho \vec{g}$$
$$\rho \overrightarrow{\nabla} \cdot \vec{U} = 0 \quad (5)$$

To inhibit the convection in the solid part of the domain, Darcy damping force was applied to the domain [8]

$$\vec{F}_D = K_{ip}\vec{U} \quad (6)$$

where $\vec{U}$ is the velocity field

$$\vec{U} = \begin{cases} u \\ v \\ w \end{cases} \quad (7)$$

and K_{ip} is an isotropic permeability defined as:

$$K_{ip} = \frac{-C(1-f_l)^2}{(f_l^3+b)} \quad (8)$$

with constants C = $1 \cdot 10^6$, b = $1 \cdot 10^{-3}$ and f_l - numerical fraction of liquid that turns to 1 when the temperature becomes equal to the melting point T_f (K):

$$f_l = flc2hs\big(T - (T_f - dT), dT\big) \quad (9)$$

At the top surface of the domain, the recoil pressure [9] was applied:

$$P_r = \left(\frac{1+\beta_r}{2}\right) P_{sat} \quad (10)$$

with pressure of saturated vapor given as :

$$P_{sat} = P_0 \, exp\left[\frac{L_{vap}\, M}{R}\left(\frac{1}{T_{vap}} - \frac{1}{T}\right)\right] \quad (11)$$

The surface tension σ (N/m) was given as :

$$\sigma = \sigma_f + \gamma T \quad (12)$$

where σ_f (N/m) is the surface tension at fusion temperature and γ is a temperature coefficient of surface tension (N/(m·K)). Surface tension was taken into consideration through Laplace equation [10] :

$$p\cdot\vec{n} = -\sigma\frac{\partial\vec{t}}{\partial s} \quad (13)$$

where $\vec{t}$ is the tangent vector to the free surface *s*.

Finally, a thermocapilary convection was taken into account:

$$\left\{-p[I] + \mu\left[\nabla\vec{U} + \left(\nabla\vec{U}\right)^T\right]\right\}\vec{n} = \gamma\overrightarrow{\nabla_t}T \quad (14)$$

2.3. Moving mesh

The free mesh displacement was solved with ALE method using Yeoh smoothing. The normal velocity of top surface $\overrightarrow{V_n}$ was formulated as:

$$\overrightarrow{V_n} = \overrightarrow{V_l} + \overrightarrow{V_g} \quad (15)$$

where $\overrightarrow{V_l}$ is the local velocity field of the melted metal

$$\overrightarrow{V_l} = u\overrightarrow{n_x} + v\overrightarrow{n_y} + w\overrightarrow{n_z} \quad (16)$$

and $\overrightarrow{V_g}$ is the velocity of vaporization front

$$\overrightarrow{V_g} = \frac{(1-\beta_r)P_{sat}\sqrt{\frac{M}{2\pi RT}}}{\rho}\vec{n} \quad (17)$$

The progressive stiffening of the meshes was introduced to avoid mesh inversion under the tip of the keyhole:

$$S = s_{const}\,[flc2hs(abs(dZ) - 5e^{-4}, 2e^{-4}) + 2\cdot flc2hs(abs(dZ) - 1.5e^{-4}, 2e^{-4})] \quad (18)$$

2.4. Materials properties

The shift of physical properties across the joint line was programmed using smoothed Heavisde functions vertically dividing the domain in two equal parts corresponding to the material 1 and material 2:

$$A = A_{M1} + (A_{M2} - A_{M1})\, flc2hs(x - 0, dx) \quad (19)$$

where $A = \ a, \rho, C_p^{eq}, k, \mu_l \ \ \sigma, \gamma, P_{sat}, L_{vap}$.

The mixing process between the materials was not considered in this study.

For each material, the physical properties were introduced as Heaviside functions of temperature, with T-dependent expressions for solid and liquid state:

$$k = k_s + (k_l - k_s)\, flc2hs\big(T - T_f, dT\big)$$
$$\rho = \rho_s + (\rho_l - \rho_s)\, flc2hs\big(T - T_f, dT\big) \quad (20)$$

The latent heat of fusion of individual material L_f(J/kg) was taken in account by means of equivalent enthalpy approach [11]:

$$C_p^{eq} = C_p^s + \left(C_p^l - C_p^s\right) flc2hs\big(T - T_f, dT\big) + L_f \frac{exp^{\frac{-(T-T_m)^2}{dT^2}}}{\sqrt{\pi\, dT^2}} \quad (21)$$

During the preliminary calculations, it was found that the combination of Darcy damping force with equivalent viscosity approach provides better numerical convergence. For this reason, the mean value of 100 Pa·s was conserved for the solid material, and the viscosity of liquid phase was applied for the temperatures ≥ T_f.

$$\mu = \mu_s + (\mu_l - \mu_s)\, flc2hs\big(T - (T_f - dT), dT\big) \quad (22)$$

3. Use of COMSOL Multiphysics® Software

The 2 x 3 x 2.5 mm^3 calculation domain (**Figure 1**) was meshed with tetrahedral elements of 250 µm maximal size, with demi-circle and rectangular boundaries meshed with 40-50 µm maximal size.

The strong coupling between the Heat transfer in fluids, laminar Navier-Stokes and Moving Mesh modules was applied. The model was solved with time-dependent solver MUMPS on the workstation with Intel ® Xeon ® CPU E5-2699v4 (2 processors, 2.2 GHz, 44 cores) and 256 Gb RAM. The longest calculation took about 10 h.

4. Experiment

The experiments were performed using a Yb:YAG laser (λ =1030 nm) at a focal distance of 200 mm, focused spot diameter of 0.58 mm and pulse duration of 4 and 6 ms. Laser beam of 1.5 kW power for Ti and 2.5 kW for Al was focused at the top surface of the plate. In case of dissimilar Ti- stainless steel joint, the beam was centered on the joint line. No gas protection was used. The dimensions of the melted zone were evaluated post-mortem after the breaking of the joint and compared with calculated dimensions of the melted zone.

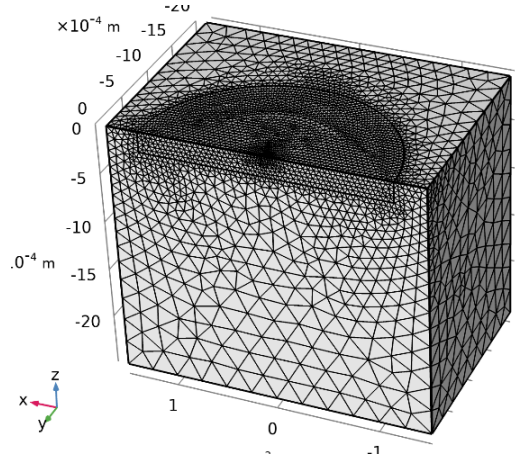

Figure 1. Geometry and mesh.

5. Results and discussion

5.1. Validation of the model

In the first place, the model was validated by the comparison with standalone laser pulses on titanium (**Figure 2**) and aluminum (**Figure 3**). Two controlled dimensions of numerical melted zone (weld penetration *H* and maximal weld width *W* shown on **Figure 2a** and **Figure 3a**) were found to be close to the experimental data in both cases (**Figure 2c, Figure 3b**). Relative errors on *H* did not exceed 20% for both materials, when relative errors on *W* were at maximum 10 % for titanium and only 5% for aluminum.

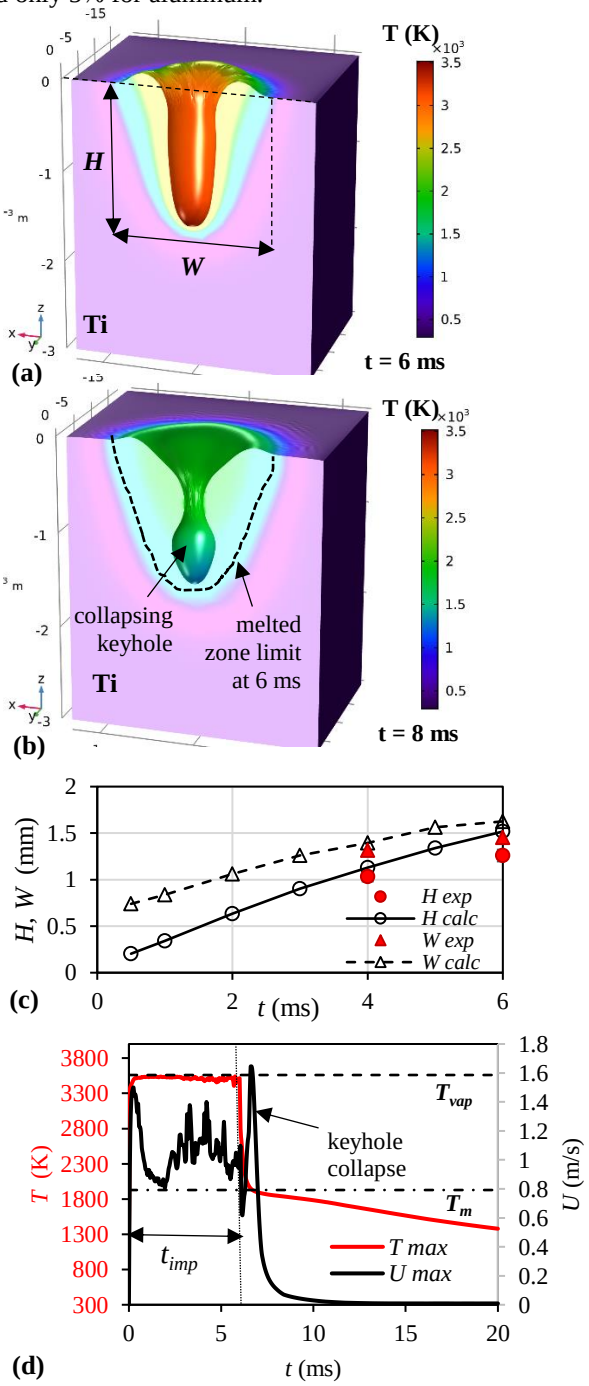

Figure 2. Model validation on titanium (1.5 kW, 6 ms) : the melted zone at the end of the pulse (a) and after the collapse of the keyhole (b); comparison with experimental dimensions (c); evolution of maximal temperature and liquid velocity (d).

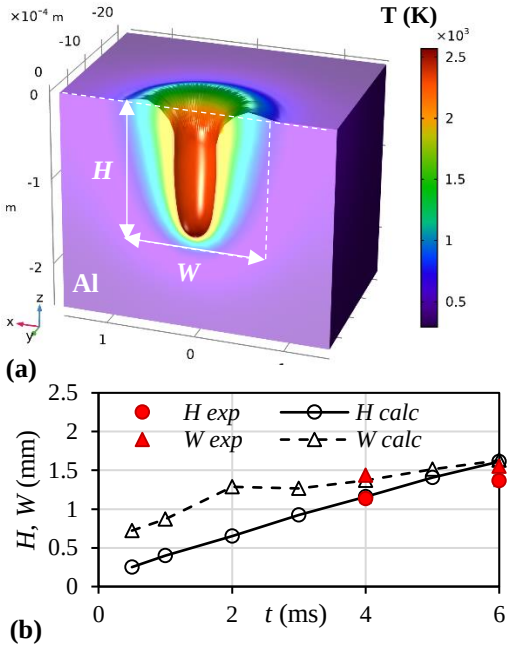

Figure 3. Model validation on aluminum (2.5 kW, 6 ms) : the melted zone at the end of the pulse (a); the comparison with experiment (b).

The maximal temperature in the impact zone was situated at the bottom of the keyhole, where the main mass loss through evaporation took place. The keyhole was surrounded by a donut-like ring of melted material that partially collapsed inside the keyhole after the end of the pulse (**Figure 2b**). The ALE method does not allow simulating a complete trapping of the keyhole because the coalescence of meshes of the keyhole walls is not possible. However, the model showed quite well the moment before the closing of the liquid walls above the keyhole root.

The evolution of maximal temperature and velocity field in the impact zone is illustrated by the case of titanium (**Figure 2d**). The sharp increase of surface temperature at the beginning of the pulse up to the boiling temperature of material was followed by a plateau until the end of the pulse and ended by a rapid decrease down to the melting temperature. The solid material underwent slow cooling that was not achieved during the calculation time of 20 ms. The velocity of melted material did not exceed 2 m/s and was maximal during the initiation of the melt and the collapse of the keyhole. The residual liquid velocity observed below the melting temperature was determined by the value of smoothing interval dT = 200 K that controls the local fraction of liquid (equation 9) and the value of 100 Pa·s for equivalent viscosity of the solid (equation 22) optimized for the better convergence.

In the second place, the model was applied to the dissimilar couple titanium-stainless steel. Titanium has a vaporization temperature about 520 K higher than stainless steel, but also about 10% higher absorptivity of laser radiation. Consequently, the developing keyhole is almost symmetrical, with its root slightly displaced towards titanium (**Figure 4a**). The walls of the keyhole from each side of the joint have different temperatures that match with vaporization temperatures of the materials at normal pressure. After the end of the pulse, the mismatch in density, viscosity and surface tension produces an asymmetrical collapse of the ring of melted matter, with formation of a trapped keyhole.

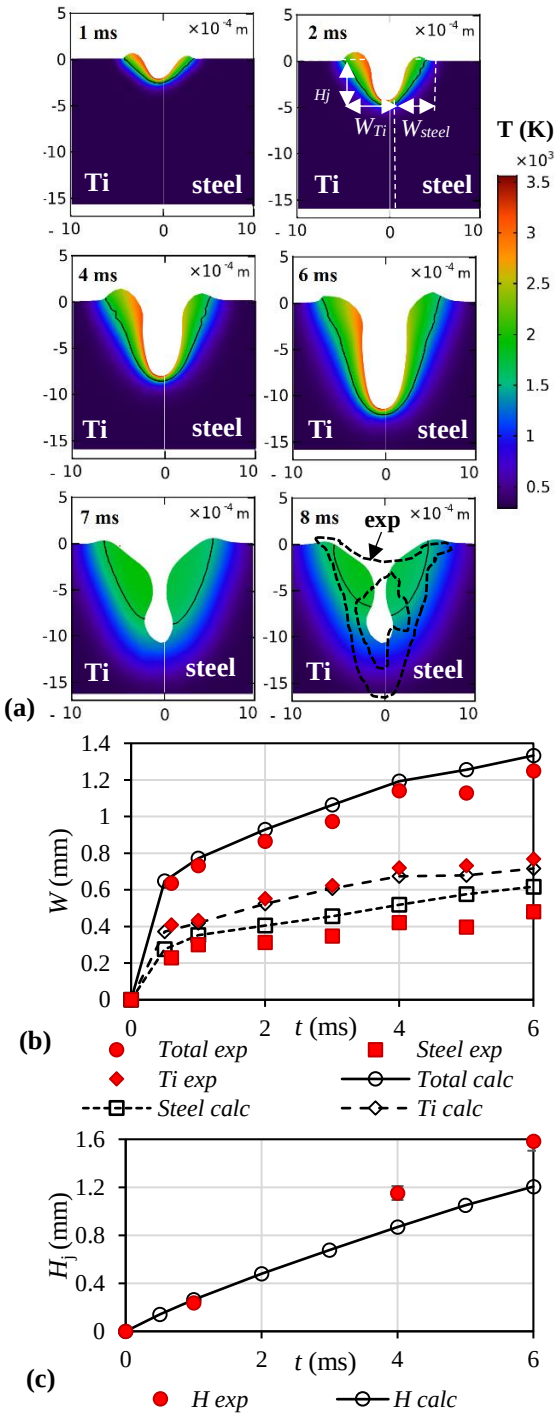

Figure 4. A case of dissimilar titanium-steel couple (1.5 kW, 6 ms): the evolution of impact zone (a), the validation of experimental widths of the melted zone (b) and the weld penetration at the joint line (c).

The calculated width of the melted zone on titanium and steel sides was compared with the dimensions observed during high-speed imaging [6] (**Figure 4b**). Slight overestimation of melting on the steel side was observed, possibly due to the inexact data on the recoil pressure of steel. The progression of melted zone width (W_{total}) was estimated with error ≤10 %. The calculated penetration at the joint line (H_j) was at maximum 24% lower than experimental one (**Figure 4c**), but this difference can be also be due to the microscopic gap between the plates that would facilitate the digging of the melted zone. Because of the loss of matter through evaporation, the solidified impact zone had a convex profile and the broken sample contained the bubbles due to the trapped keyhole (shown by black dash lines at 8 ms image of **Figure 4a**). The final state of the calculated free surface presented the identical convex profile and partially trapped keyhole.

5.2. Evaluation of keyhole asymmetry

Basing on sparse literature data [1-5], it can be supposed that the mismatches in vaporization temperatures and absorption coefficients are the main factors of keyhole asymmetry in dissimilar welding. To investigate their effect, two sets of dissimilar joints composed by a reference metal M1 and a random opposite metal M2 were considered. In the first set, the reference metal M1 was titanium that has quite high absorption coefficient (40%) and in the second, it was highly reflective copper (3%). The random metals (M2) were chosen in order to obtain a wide range of vaporization temperatures (Table 1) and did not contain any highly reflective materials like gold, copper etc.

The Yb:YAG laser beam with diameter of 0.58 mm, laser power 1.5 kW and pulse duration of 6 ms, centered on the joint line was considered in all calculations.

The asymmetry of the keyhole was quantified by two characteristics: the relative keyhole section in the reference material M1

$$A_s^{M1}(\%) = \frac{S_{M1}}{S_{M1}+S_{M2}} \cdot 100 \qquad (23)$$

where S_{M1} and S_{M2} are the keyhole sections in M1 or M2 measured at the end pulse on the symmetry plane, and the relative root offset :

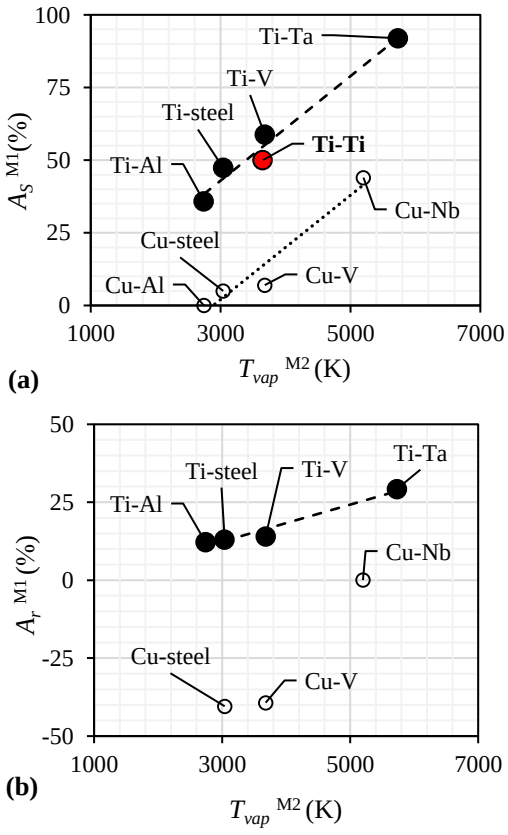

Figure 5. Evolution of (a) relative keyhole section and (b) relative root offset (1.5 kW, 6 ms).

$$A_r^{M1}(\%) = \frac{\Delta_{M1}}{R_l} \cdot 100 \quad (24)$$

where Δ_{M1} is the offset of the keyhole root to the joint line, considered as positive in M1 and negative in M2 and R_l is the radius of the laser spot.

For a homogenous joint, for example Ti-Ti, $A_s^{Ti}(\%) = 50$ %. In standalone copper the keyhole does not form. The root offset from the joint line is observed only in dissimilar couples.

For both Ti-containing and Cu-containing couples, the linear increase of relative keyhole section in M1 along with vaporization temperature of M2 was observed (**Figure 5a**). In case of Ti-containing welds, for the metals having $T_{vap}^{M2} < T_{vap}^{Ti}$, the keyhole was formed preferentially in M2 (**Figure 6a**), was equally shared in case of $T_{vap}^{M2} \approx T_{vap}^{Ti}$ (**Figure 6b**) and formed preferentially in titanium for $T_{vap}^{M2} > T_{vap}^{Ti}$ (**Figure 6c-d**). Because of high reflectivity and high thermal diffusivity of copper, it is much more complicated to shift the keyhole from M2 on copper, even for the metals with high T_{vap}^{M2} (**Figure 5a**). In case of materials having $T_{vap}^{M2} \leq T_{vap}^{Cu}$, the melted zone is formed only on M2 side, and the creation of the keyhole is strongly inhibited by high thermal diffusivity of neighboring copper (**Figure 7a**). For $T_{vap}^{M2} > T_{vap}^{Cu}$, the progressive increase of vaporization temperature of M2 allows involving the copper side into the keyhole (**Figure 7b-d**), however, the formation of symmetric keyhole can be attained only for $T_{vap}^{M2} > 5000$ K. One should remember that such behavior of copper is typical for low energy densities, and the keyhole can actually shift on copper side [**Erreur ! Signet non défini.**] when using more intense laser radiation (even Yb:YAG) in combination with material having higher boiling point (such as stainless steel). The additional study should be performed for Cu-containing welds to demonstrate the evolution of keyhole asymmetry with increasing laser power.

The relative root asymmetry of Ti-containing welds (**Figure 5b**) shows a linear increase with T_{vap}^{M2}. The root asymmetry is never negative, which means, the keyhole root is always shifted towards titanium and approaches $R_l/2$ for $T_{vap}^{M2} > 5000$ K. For Cu-containing welds, on contrary the root asymmetry is negative, which means, the root of the keyhole is systematically shifted on M2 closely to $R_l/2$ value. The root returns to the joint line only for $T_{vap}^{M2} > 5000$ K.

The vertical offset between all titanium and copper correlations (**Figure 5**) is likely to be determined by the sharp mismatch in laser absorption coefficients between copper and titanium.

Table 1. Vaporization temperatures of metals (K).

Cu	Al	S.s.	Ti	V	Nb	Ta
2835	2792	3013	3560	3680	5017	5731

6. Conclusions

The ameliorated auto-consistent ALE-based multiphysical model of transient evolution of laser melted zone in metallic materials was proposed. It involves strong coupling between Heat transfer equation including heat loss through evaporation, laminar Navier-Stokes equation combining Darcy damping force and equivalent viscosity approach and ALE problem with Yeoh smoothing.

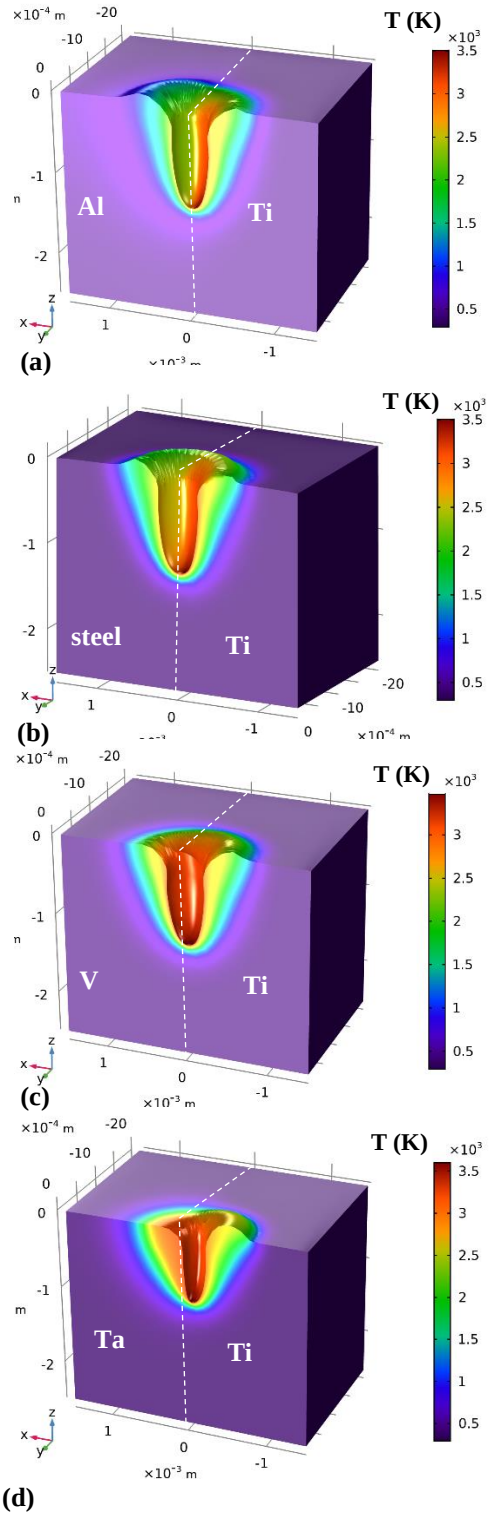

Figure 6. Thermal field in Ti-containing dissimilar welds (1.5 kW, 6 ms).

The model showed a satisfactory correspondence with experimental dimensions of the melt in case of standalone and dissimilar pulsed laser welding. It allows adequate representation of gradual keyhole development and collapse after the end of the pulse.

The model was used for the comprehension of keyhole asymmetry in dissimilar butt joints welded by a pulsed laser. The asymmetry of the keyhole due to the mismatch in

vaporization temperatures between welded reference metal and neighboring random metal was quantified through two variables: relative keyhole section and relative root offset. The linear increase of keyhole section in a reference material in function of vaporization temperature of a random material was generally observed, but it appears to be much lower in case of highly reflective reference material such as copper.

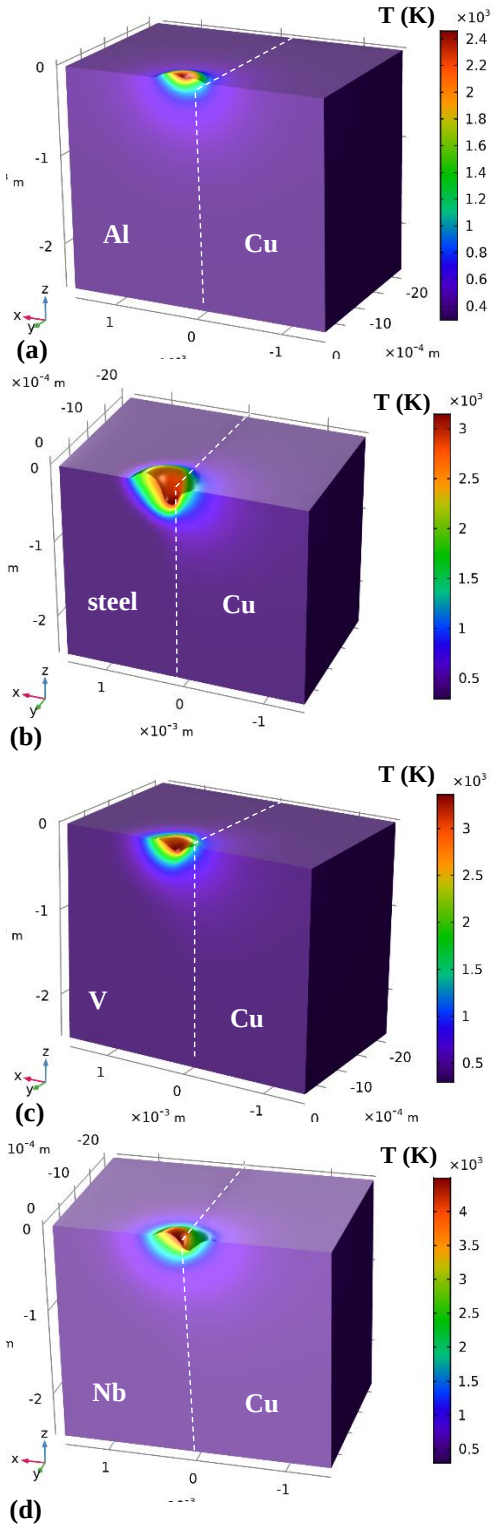

Figure 7. Thermal field in Cu-containing dissimilar welds (1.5 kW, 6 ms).

The position of keyhole root is strongly determined by the reflectivity of reference material: in case of copper, the keyhole root is usually shifted towards the opposite material, and returns on the joint line only in case very high vaporization temperature of the opposite material. In case of well-absorbing material such as titanium, the keyhole root remains on a reference side and shifts away from the joint line with increase of vaporization temperature of a random material.

7. References

[1] M.J. Torkamany, F. Malek Ghaini, R. Poursalehi, An insight to the mechanism of weld penetration in dissimilar pulsed laser welding of niobium and Ti-6Al-4V, *Optics and Laser Technology*, **79**, 100-107 (2016).

[2] D. Grevey, V. Vignal, I. Bendaoud, P. Erazmus-Vignal, I. Tomashchuk, D. Daloz, P. Sallamand, Microstructural and micro-electrochemical study of a tantalum–titanium weld interface, *Materials & Design*, **87**, 974-985 (2015).

[3] I. Tomashchuk, M. Mostafa, T. Caudwell, P. Sallamand, M. Duband, Behavior of laser induced keyhole during dissimilar welding of metals, *Lasers in Manufacturing Conference 2017*, June 26-29, Munich, Germany (2017).

[4] I. Tomashchuk, M. Mostafa, T. Caudwell, P. Sallamand, M. Duband, Formation du capillaire de vapeur lors de l'interaction de laser de puissance avec la jonction dissimilaire Al-Mg, *Congrès Français de Thermique 2017*, 30 mai – 2 juin, Marseille, France (2017).

[5] I. Tomashchuk, Assemblage hétérogène cuivre-inox et TA6V-inox par les faisceaux de haute énergie : compréhension et modélisation des phénomènes physico-chimiques, phD thesis at Université de Bourgogne, France (2010). http://www.theses.fr/2010DIJOS055

[6] I. Tomashchuk, I. Bendaoud, P. Sallamand, E. Cicala, S. Lafaye, M. Almuneau, Multiphysical modelling of keyhole formation during dissimilar laser welding, *Conference COMSOL 2016*, 12-14 October 2016, Munich, Germany.

[7] C. J. Knight, Theoretical modeling of rapid surface vaporization with back pressure, *American Institute of Aeronautics and Astronautics Journal*, **17:5**, 19–523 (1979).

[8] M. Courtois, M. Carin, P. Le Masson, S. Gaied, M. Balabane. A complete model of keyhole and melt pool dynamics to analyze instabilities and collapse during laser welding. *Journal of Laser Applications*, **26:4**, 042001 (2014).

[9] R. Fabbro, K. Chouf, Dynamical description of the keyhole in deep penetration laser welding, *Journal of Laser Applications*, **12:4**, 142-148 (2000).

[10] E. Guyon, J.P. Hulmin, L. Petit, *Hydrodynamique Physique*, Edition du CNRS (1994)

[11] C. Bonacina, G. Comini, A. Fassano, M. Primicerio, Numerical solutions of phase change problems, *International Journal of Heat Mass Transfer*, **16**, 1825-1832 (1973).

8. Acknowledgements

This work was carried out as a part of a joint laboratory project LabCom FLAMme between *Laboratoire Interdisciplinaire Carnot de Bourgogne*, *University of Bourgogne-Franche-Comté* and *SME Laser Rhône-Alpes*. This project was supported by French National Agency of Research (grant number ANR-14-LAB3-0005).